

Assimilation of GOME ozone profiles and a global chemistry-transport model, using a Kalman Filter with anisotropic covariance

By A. J. SEGERS^{1*}, H. J. ESKES¹, R. J. VAN DER A¹, R. F. VAN OSS¹, and P. F. J. VAN VELTHOVEN¹

¹*Royal Netherlands Meteorological Institute (KNMI), The Netherlands*

(Received 14 June 2004; revised 9 October 2004)

SUMMARY

Nadir ozone profiles retrieved from the GOME (Global Ozone Monitoring Experiment) instrument are assimilated with a global three-dimensional atmospheric ozone model. The assimilation procedure is based on the Kalman filter equations, and is an extension of an existing assimilation procedure for total ozone columns. As a novelty, a three-dimensional covariance model is developed using a single parameterisation for correlations in all directions, instead of the usually applied separation in horizontal and vertical directions. The parameterisation is anisotropic in all directions, accounting for the different correlation lengths of ozone with respect to altitude, latitude, and longitude. The assimilation procedure includes full use of the averaging kernel information provided with the GOME retrieval product. The averaging kernels account for the smaller sensitivity of the GOME instrument below the ozone maximum and the limited vertical resolution. A singular value decomposition of the kernels is used to reduce the large data volume. A one year data set of GOME ozone profiles is assimilated for the year 2000. Independent data from ozone sondes is used to validate the results. A case study shows that the assimilation of GOME profiles is able to improve the simulation of the vertical ozone distribution even in case of strong vertical gradients.

KEYWORDS: ozone sondes averaging kernels

1. INTRODUCTION

A detailed knowledge of ozone is important for atmospheric chemistry and climate research (IPCC 2001; WMO 2003; EC 2003). Ozone absorbs harmful uv-radiation, plays a central role in the chemistry of smog formation, and contributes to global warming as a greenhouse gas. Numerical weather prediction centres are interested in ozone for the heating of the atmosphere by the stratospheric ozone layer. On a time scale of hours to days, ozone may also be useful as a passive tracer to derive stratospheric wind vectors (Riishøjgaard 1997).

Ozone has been observed by several satellite instruments over the last decades. The longest time series of total ozone columns is provided by the TOMS (Total Ozone Mapping Spectrometer) instruments, and forms an almost continuous record since the end of the seventies. The total ozone columns measured by TOMS and more recent nadir viewing instruments as GOME (Global Ozone Monitoring Experiment, (Burrows *et al.* 1999)) have provided valuable information on stratospheric ozone, in particular on Antarctic ozone depletion. Information on the vertical distribution of ozone is required for the study of stratosphere/troposphere exchange, formation and breakup of the polar vortex, and, ultimately, the tropospheric and stratospheric ozone budgets. Vertical information has been provided by the nadir viewing SBUV/SBUV2 (Solar Backscatter UV) instruments, operational since the end of the seventies. The SBUV measurements provide information on the ozone profile with a resolution of roughly 8 km in the upper stratosphere, between 25 and 45 km. Limb-viewing instruments such as MLS (Microwave Limb Sounder) and occultation instruments such as HALOE (HALogen Occultation Experiment), SAGE (Stratospheric Aerosol and Gas Experiment), or POAM (Polar Ozone and Aerosol Measurement), provide ozone profiles with a higher vertical resolution and accuracy, but these measurements are characterised by a low horizontal resolution or coverage.

* Corresponding author: Atmospheric Composition Division, Royal Netherlands Meteorological Institute (KNMI), P.O. Box 201, 3730 AE De Bilt, The Netherlands.

© Royal Meteorological Society, 2004.

The GOME instrument improves on both TOMS and SBUV through its better spectral resolution and coverage, respectively. The earth-shine spectrum measured by GOME contains more profile information than the SBUV spectrum, especially in the lower stratosphere and the troposphere. GOME ozone profile retrieval algorithms have been reported by Munro *et al.* (1998), Hoogen *et al.* (1999), Hasekamp and Landgraf (2001), and Van der A *et al.* (2002). The vertical resolution of these retrieval techniques is about 5 km around the ozone maximum and worse below and above. The ability of the instrument to infer the vertical ozone distribution is described by the averaging kernels of the retrieval. These provide the relation between the true and the retrieved profile. To correctly interpret the retrieved ozone profiles, it is essential to take into account the averaging kernels when comparing with model simulations or sonde measurements (Meijer *et al.* 2003).

Ozone measurements are nowadays assimilated by various research groups and operational weather forecast centres. The KNMI (Royal Netherlands Meteorological Institute) has been providing daily global ozone forecasts since early 2000 based on assimilation of total ozone from GOME (Eskes *et al.* 2003), and currently does so based on SCIAMACHY (SCanning Imaging Absorption spectroMeter for Atmospheric CartograpHY). The ECMWF (European Centre for Medium-range Weather Forecasts) assimilated TOMS total ozone and SBUV data during the 40-year reanalysis (Dethof and Hólm 2002), and has recently started to provide ozone forecasts as an operational product, first based on GOME, SBUV and MIPAS (Michelson Interferometer for Passive Atmospheric Sounding) data, and currently SCIAMACHY measurements. NASA's Global Modelling and Assimilation Office (GMAO) assimilates TOMS and SBUV data offline in GEOS (Goddard Earth Observing System) (Štajner *et al.* 2001). Limb measurements from MLS have been assimilated by for example Levelt *et al.* (1998), Khattatov *et al.* (2000), Struthers *et al.* (2002), and Fierli *et al.* (2002). Ozone assimilation as part of more extensive chemical analysis has been performed in various studies. A variational approach for assimilation of multiple stratospheric trace gas observations was introduced in Fisher and Lary (1995), and later on applied by for example Errera and Fonteyn (2001). Elbern and Schmidt (2001) applied the variational approach for regional air pollution forecasts.

This paper describes the assimilation of GOME ozone profiles and a global atmospheric ozone model. The aim is to build an assimilation system that is able to provide the best possible three dimensional fields of ozone based on profiles measured by GOME, and in future its successors. In an online application, such an assimilation system would be able to provide more information on the vertical distribution of ozone than the current ozone forecast systems, that assimilate total ozone columns only. High quality stratospheric ozone fields form also the key data for retrieving tropospheric ozone data from satellite instruments. In addition, an assimilation system is useful to quantify the uncertainty of the observation. This knowledge may initiate improvements in the satellite retrievals.

The assimilation system described in this study is based on the existing total ozone column assimilation described in Eskes *et al.* (2003) and the experiences with ozone profile assimilation described in El Serafy and Kelder (2003). The first step to be made when developing such a system is to study the quality of the satellite profiles. Biases between the profiles and model simulations should be identified, as well as the overall uncertainty in the profiles with respect to location, altitude, and season. The second step is to construct an analysis system that makes optimal use of the information present in the ozone profile retrievals. Important issues are the modelling of vertical correlations,

the treatment of the averaging kernels in the profile product, and efficiency in view of the large data volume.

The assimilation system is based on the Kalman filter. An atmospheric model and the GOME measurements are the most important components of the system, together with other elements such as a covariance model and an observation operator. Since the components of the system are closely related to each other, it is fairly impossible to introduce one component without having a modest idea about the others. The Kalman filter equations are therefore summarised first in section 2. The components of the system are then described in more detail: the atmospheric model (section 3), the covariance model (section 4), the forecast equations of the Kalman filter (section 5), the ozone profiles retrieved from GOME (section 6), the observation operator simulating ozone profiles from the model state (section 7), and the analysis equations of the Kalman filter (section 8). A one-year data set of GOME ozone observations is assimilated for the year 2000. Section 9 describes the resulting assimilated ozone data set and the error statistics obtained by comparison with sonde measurements.

2. KALMAN FILTER - INTRODUCTION

The aim of a data assimilation system is to obtain the best possible estimate of the true state, given measurements and all previous knowledge of the evolution of the state and known constraints on the state vector. In particular, the Kalman filter provides the best estimate of a state at a certain time, given all measurements that have become available up to that time and the physical constraints implemented in a model.

Let $\mathbf{x}^{[k]}$ denote the true state of the atmosphere, described in a vector, defined for the time t_k . In this study, \mathbf{x} describes the global ozone concentration field. Further, let $\mathbf{y}^{[k]}$ denote a vector of measurements. The first step in the implementation of a Kalman filter is to identify models for the atmosphere and the measurements. They have the general form

$$\mathbf{x}^{[k]} = M(\mathbf{x}^{[k-1]}, t_{k-1}, t_k) + \mathbf{w}^{[k-1]} \quad , \quad \mathbf{w}^{[k-1]} \sim \mathcal{N}(\mathbf{o}, \mathbf{Q}^{[k-1]}) \quad (1a)$$

$$\mathbf{y}^{[k]} = H(\mathbf{x}^{[k]}, t_k) + \mathbf{v}^{[k]} \quad , \quad \mathbf{v}^{[k]} \sim \mathcal{N}(\mathbf{o}, \mathbf{R}^{[k]}) . \quad (1b)$$

Equation (1a) describes the evolution of the state from t_{k-1} to t_k with the aid of the model M . In our study, the model is the global atmospheric chemistry model TM3 (Transport Model, version 3), described in detail in section 3. Since a model is never perfect, the true state $\mathbf{x}^{[k]}$ will not be equal to $M(\mathbf{x}^{[k-1]})$, even if $\mathbf{x}^{[k-1]}$ would be known exactly. The error made by the model is represented by the stochastic vector \mathbf{w} , which is supposed to have a normal distribution (\mathcal{N}) with zero mean \mathbf{o} and covariance \mathbf{Q} . We will not implement the model error covariance \mathbf{Q} directly, but rather use a parameterisation for the operation in which \mathbf{Q} is involved. Measurement vector \mathbf{y} contains the measured data, in our case the GOME ozone profiles. The information content of \mathbf{y} is described in section 6. Representation operator H describes how the measured data can be derived from the state vector. For the analysis step in the Kalman filter it is necessary to have a linearisation of H around an a-priori state \mathbf{x}^0 of the form

$$H(\mathbf{x}, t_k) \approx H(\mathbf{x}^0, t_k) + \mathbf{H}^{[k]} (\mathbf{x}^{[k]} - \mathbf{x}^0) \quad (2a)$$

$$= H_0^{[k]} + \mathbf{H}^{[k]} \mathbf{x}^{[k]} . \quad (2b)$$

The actual measurements \mathbf{y} will differ from $H(\mathbf{x})$ because \mathbf{x} is only a discrete representation of the true atmosphere where the measurement is taken, our model H of the measurement technique may not be perfect, and because of random measurements errors

of the instrument. The difference is described by a stochastic vector \mathbf{v} which is assumed to be unbiased (zero mean) and to have a known covariance \mathbf{R} . The representation operator H , the error covariance \mathbf{R} , and the assumption of an unbiased error are discussed in section 7.

In the context of the Kalman filter, the range of most likely values that the true state can have is expressed in terms of a Gaussian probability distribution. A Gaussian probability distribution is completely defined by a mean and covariance, here denoted by $\bar{\mathbf{x}}$ and \mathbf{P} respectively:

$$\mathbf{x}^{[k]} \sim \mathcal{N}(\bar{\mathbf{x}}^{[k]}, \mathbf{P}^{[k]}) \quad (3)$$

The implementation of a full covariance matrix \mathbf{P} is in practice computationally far too expensive. The emphasis of this article is therefore on the parameterisation of \mathbf{P} , which is described in detail in section 4.

The Kalman filter computes the best estimate of the mean and covariance at a certain time in two steps. The *forecast* step computes a mean and covariance given the latest mean and covariance and other entities available for a previous time:

$$\bar{\mathbf{x}}^f_{[k]} = \mathbf{E}[\mathbf{x}^{[k]} | t_{k-1}] \quad (4a)$$

$$\mathbf{P}^f_{[k]} = \mathbf{E}\left[(\mathbf{x}^{[k]} - \bar{\mathbf{x}}^{[k]})(\mathbf{x}^{[k]} - \bar{\mathbf{x}}^{[k]})^T | t_{k-1}\right] \quad (4b)$$

where $\mathbf{E}[\cdot]$ denotes the expectation. The *analysis* step computes a conditional mean and covariance given measurement data, as soon as this becomes available:

$$\bar{\mathbf{x}}^a_{[k]} = \mathbf{E}[\mathbf{x}^{[k]} | \mathbf{y}^{[k]}] \quad (5a)$$

$$\mathbf{P}^a_{[k]} = \mathbf{E}\left[(\mathbf{x}^{[k]} - \bar{\mathbf{x}}^a_{[k]})(\mathbf{x}^{[k]} - \bar{\mathbf{x}}^a_{[k]})^T | \mathbf{y}^{[k]}\right]. \quad (5b)$$

The forecast equations are described in detail in section 5 after description of model and covariance, and the analysis equations in section 8 after description of observations and observation model.

3. ATMOSPHERIC CHEMISTRY MODEL

The atmospheric model with parameterised ozone chemistry used in this study is adapted from the global atmospheric chemistry model TM3 (Transport Model, version 3), as described by Eskes *et al.* (2003).

TM3 is an off-line model driven by meteorological fields from ECMWF (Bregman *et al.* 2003). The horizontal resolution is $3^\circ \times 2^\circ$ deg. (lon \times lat). In the vertical, the model has 44 hybrid sigma-pressure layers with a top at 0.1 hPa. The sigma-pressure levels considered are a subset of ECMWF's operational 60 layer configuration. In the stratosphere, the levels match exactly with the ECMWF levels, while in the troposphere, some of the original layers are combined. The choice of vertical levels is related to the focus of the assimilation on producing accurate stratospheric ozone fields.

The stratospheric ozone formation and loss is parameterised using a simple gas-phase chemistry (Cariolle and Déqué 1986, McLinden *et al.* 2000) and a heterogeneous chemistry based on chlorine activation, the so-called 'cold tracer' scheme (Hadjinicolaou and Pyle 2004). Tropospheric chemistry is not included; instead, the tropospheric ozone profile is relaxed toward a climatology (Fortuin and Kelder, 1998) with a long relaxation time scale of two weeks. A simple deposition term accounts for the ozone loss at the surface.

4. COVARIANCE MODEL

The covariance matrix describes the probability of the true state \mathbf{x} to be different from our best estimate $\bar{\mathbf{x}}$:

$$\mathbf{P}^{[k]} = \mathbf{E} \left[(\mathbf{x}^{[k]} - \bar{\mathbf{x}}^{[k]})(\mathbf{x}^{[k]} - \bar{\mathbf{x}}^{[k]})^T \right]. \quad (6)$$

The dimension of the covariance matrix \mathbf{P} is large: the square of the number of elements in the state \mathbf{x} . For large atmospheric models such as used for ozone simulations it is practically impossible to work with or even to store a full covariance matrix. Lyster *et al.* (1997) implemented a Kalman filter for an atmospheric model with full covariance, but only with the aid of massive parallel computing. A number of methods can be applied to deal with the size problem.

The dimension of the covariance matrix can for example be reduced by defining it in a space of reduced dimension, for example on a reduced grid, or in two rather than three dimensions. An interpolation routine should map the reduced field back to the original state. In Eskes *et al.* (2003) for example, ozone column measurements are analysed in two dimensions. The resulting ozone column analysis was subsequently distributed over the vertical layers proportional to the ozone profile.

Another method to reduce the size of \mathbf{P} is to parameterise its contents. The covariance between two state elements can for example be described by their standard deviations and a spatial correlation based on their distance. El Serafy and Kelder (2003) neglected the spatial correlations and implemented a simplified Kalman filter for the analysis of GOME profiles that analysed the variance field only. In Eskes *et al.* (2003), the spatial correlation in total ozone was parameterised as a function of the horizontal distance. A 3D parameterisation is described in Štajner *et al.* (2001), based on horizontal distance and vertical pressure differences. An elegant method is used to make the horizontal correlations anisotropic, by applying a geometrical transformation that projected the earth's surface on a new body. The use of anisotropic correlation models becomes more and more popular, since it accounts for the differences in correlation lengths with respect to latitudinal and vertical position and direction. In (Riishøjgaard 1998) for example, flow dependent correlations were constructed by measuring distances in terms of differences in potential temperature and potential vorticity rather than location.

In this study, a full 3D anisotropic covariance matrix is built following the concept of a geometrical transformation as described in Štajner *et al.* (2001), generalised to all three dimensions. It will provide a simple parameterisation from which correlations between all possible pairs of grid points can be computed quickly.

(a) Covariance parameterisation

A suitable method to compute a covariance *matrix* is to define a continuous covariance *function* first, and then to form a matrix by evaluating the function on a discrete grid. Here we define a covariance function in the following way. Let ξ_1 and ξ_2 be two vectors pointing to locations in the atmosphere. The covariance function $P : \mathbf{R}^3 \times \mathbf{R}^3 \rightarrow \mathbf{R}$ is written in the form

$$P(\xi_1, \xi_2; t_k) = \sigma(\xi_1; t_k) C(\xi_1, \xi_2) \sigma(\xi_2; t_k) \quad (7)$$

where $\sigma : \mathbf{R}^3 \rightarrow \mathbf{R}_0^+$ is a 3D time dependent standard deviation field, and $C : \mathbf{R}^3 \times \mathbf{R}^3 \rightarrow [-1, 1]$ a constant correlation field. The chosen decomposition in standard deviation σ and constant correlation C implies that temporal changes in P are to be applied

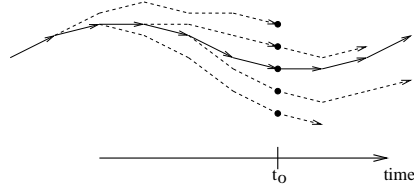


Figure 1. Illustration of the NMC method. A set of model forecasts is made for time t_0 for different time lags. The differences between the model forecasts at t_0 provide information on the correlations in the model state.

on σ rather than on C . The correlation C may be weakly time dependent however, for example different for each month.

A simple method to form a valid correlation function C is to parameterise it as a function of distance:

$$C(\xi_1, \xi_2) = \gamma(\|\xi_1 - \xi_2\|) \quad (8)$$

where $\gamma : \mathbf{R} \rightarrow [-1, 1]$ is a correlation function on \mathbf{R} , and $\|\cdot\|$ is the Euclidean norm on \mathbf{R}^3 . The correlation is thus determined by the distance between ξ_1 and ξ_2 , where the distance is the length of a straight line, possibly through the earth's interior. In this way, a covariance matrix based on evaluation of the above function is always positive definite (Gaspari and Cohn 1999).

Often, the correlation between two points does not depend on their distance only, but also depends on their position. To take this into account, a fundamental lemma of correlation function theory is used, which says that for a one-to-one transformation $\tau : \mathbf{R}^3 \rightarrow \mathbf{R}^3$ the function

$$C(\xi_1, \xi_2) = \gamma(\|\tau(\xi_1) - \tau(\xi_2)\|) \quad (9)$$

is still a correlation function. The aim is to define the transformation τ such that the distances after transformation match with the required correlation. Thus, if in a certain area of the domain the grid points are correlated strongly, their distance in transformed space should be smaller, and vice versa. The problem is thus how to shrink or stretch the original grid in such a way that the Euclidean distance between grid points becomes proportional to the correlation. In our study, the distances should represent the correlations in the ozone tracer distribution. The problem is solved by optimising the free parameters in a grid transformation such that the resulting distances represent observed correlations in ozone. The observed correlations are taken from model simulations using the NMC method, which will be explained first, followed by a description of the grid transformation.

(1) *NMC method*

The NMC method is named after the *US National Meteorological Center's* analysis system, described in (Parrish and Derber 1992). To obtain a correlation model for the error in a numerical weather model, the model should be started from different initial states, for example forecast and analysis states. Due to the different initial conditions, the model forecasts will deviate from each other (Fig. 1). The spatial scales of the differences between the model forecasts could then be used as a measure for the correlation lengths described by the model, and, as such, for the correlations in the atmosphere.

The NMC method is applied to the TM3 global ozone model described in section 3. A data base with ozone simulations is created for April 2000. For computational reasons the NMC experiment is carried out for a single month only. The month of April is chosen

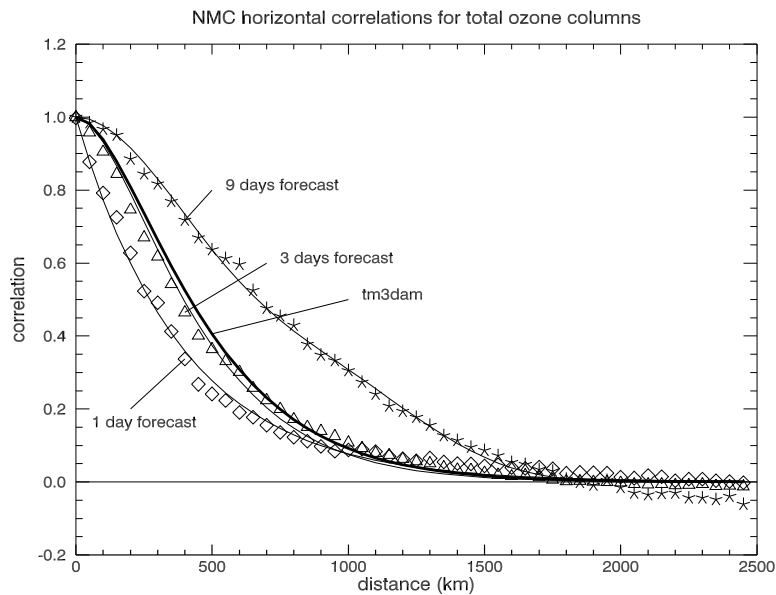


Figure 2. Horizontal correlation of total ozone as a function of horizontal distance between grid points. Derived with the NMC method, for selected forecast lags of one day, three days, and nine days. The best-fit parameterised correlation function are drawn too. The thick line is the parametrised correlation found by Eskes *et al.* (2003).

since it is a more or less average month in the atmosphere, without strong Antarctic polar vortex and other features that lead to differences between the hemispheres. For a correlation model that is constant in time and assumes hemispheric symmetry, as described later on, performing the experiment during the month April only is a suitable choice.

The NMC method consists of the following steps. A reference run is made using 6 hourly meteorological forecasts. The reference run produces for each day in March and April an initial state valid at 1200 UTC. Each of this initial states serves as the start point for a forecast run over 9 days, driven by a 9 days meteorological forecast. This provides a data base in which for each day in April a set of 9 global ozone forecasts is available. Each is valid at 1200 UTC, and is produced by model forecasts started 1 to 9 days earlier. Differences between the ozone forecasts arise due to the different meteorological inputs. The spatial scales of the differences describe correlations between the uncertainties due to imperfect dynamics; uncertainty in the chemistry parameterisation is not accounted for.

Various kinds of statistics can be derived from the data base, for example standard deviations and correlation lengths. Both standard deviations and correlation lengths grow with the forecast lag due to accumulation of differences over longer time periods. As an example, Fig. 2 shows the growth of the horizontal correlation length in total ozone for different forecast lags. Since the GOME instrument has an overpass frequency of once every three days, the statistics for a forecast lag of three days are chosen to describe the correlations in this study. This choice is validated by comparison of the correlation lengths found with the NMC method with those found by Eskes *et al.* (2003) to be optimal for assimilation of GOME total ozone, also shown in Fig. 2.

(2) Correlation model

We assume that the correlation between two ozone concentrations is a function of their latitudes, altitudes, and distance. To study the differences, the earth is divided into 15 zonal bands with a width of 12 degrees latitude each. For each of these bands, the correlations are sampled between all pairs of cells that have the same:

1. level and latitude (for horizontal east/west correlations);
2. level and longitude, with at least one cell in the considered zonal band (for horizontal north/south correlations);
3. longitude and latitude (for vertical cross correlations).

A geometrical transformation is searched that best fits the sampled correlations. An iterative process of trial and error leads to a transformation of the zonal geometry (latitude and level) into a new geometry of the following form:

- the correlation function γ in (8) is a member of the family of compactly supported correlation functions described by Gaspari and Cohn (1999), with shape parameter $a = -1.0$;
- the transformation is limited to the latitude-altitude plane, longitude is unchanged;
- the new geometry is symmetric about the equator, thus the Northern and Southern latitudes are the same;
- the vertical axis is mapped from the 44 model levels to a coordinate relative to $\log(\text{pressure})$, and is restricted to be strictly increasing with the pressure; a different axis is chosen for the equator band and for each of the 7 pairs of latitude bands opposite about the equator, leading to $8 \times 44 = 352$ unknowns;
- the latitudes of the centre of a zonal band are mapped to a new position; the new latitudes are linear functions of $\log(\text{pressure})$, leading to 2 additional unknown parameters for each pair of opposite latitude bands (14 in total);
- spline interpolation is used to map locations intermediate to the central latitudes of the bands.

The 366 unknown parameters in the transformation are optimised to obtain the best fit with the sampled correlations from the NMC experiments. Figure 3 illustrates the result. The Euclidean distances in the new geometry represent many typical features of the correlations in ozone.

- Horizontal correlations in the east/west direction (Fig. 3, lower left) as well as the north/south direction (Fig. 3, upper left) become stronger at higher model levels. Here, atmospheric dynamics is dominated by large scale horizontal motions such as planetary waves. In the new geometry, this is achieved by a taking a pressure scale along the radial axis, leading to smaller radius of the 'circles' near the origin that represent the upper atmosphere.
- The 'egg' shape with smaller radius around the equator leads to east/west horizontal correlations that are relatively stronger in the tropics than at mid latitudes (at a specific level). This represents the overall stronger east/west circulation in the tropics. A stretched latitudinal axis around the equator prevents the north/south correlations from becoming stronger too.
- Vertical correlations between levels are weaker in the stratosphere due to its greater vertical stability. In the transformed geometry, the vertical correlations are completely defined by the distances between the levels, and these are larger near the origin representing the upper atmosphere (Fig. 3, upper right).

The atmospheric volume that is correlated with a vertical profile has a cone shape, with a small radius in the troposphere and a large radius at higher altitudes (globe

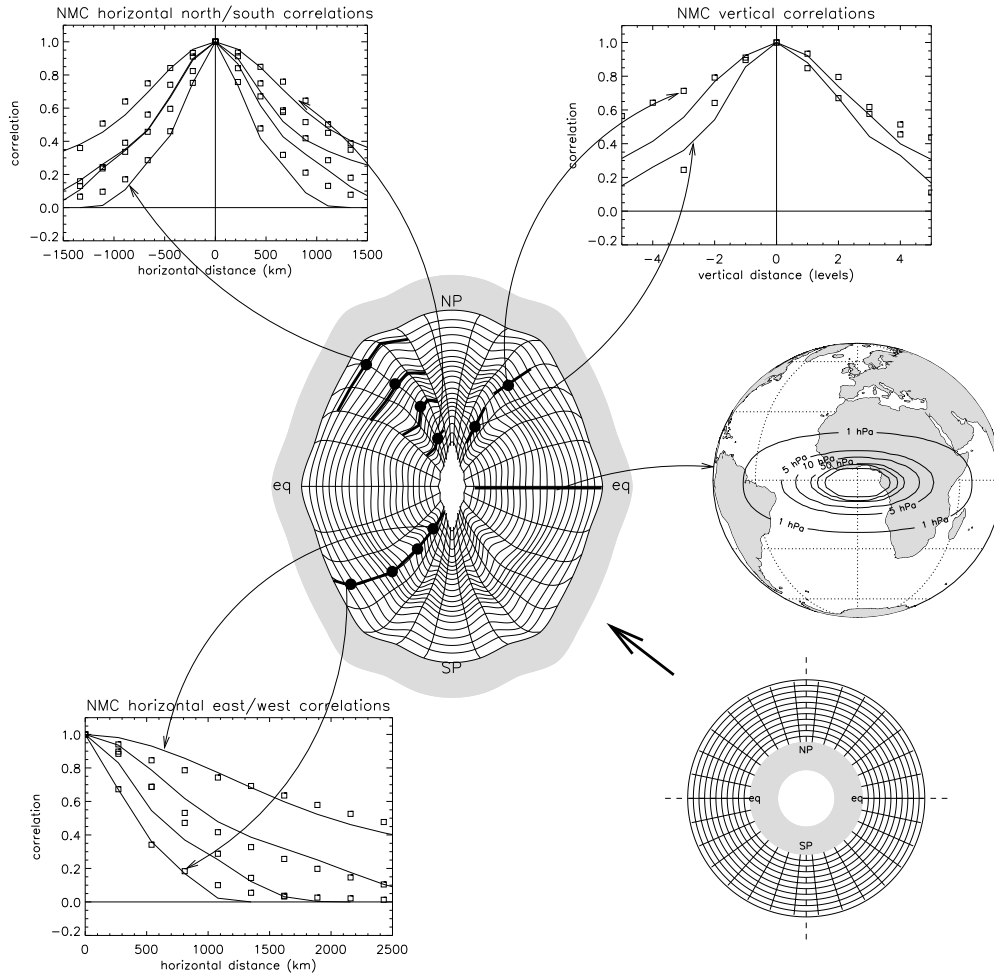


Figure 3. Illustration of the geometry used for the correlation model. The original spherical geometry is displayed in the lower right panel. In the new geometry, the radial axis has the interpretation of a pressure, leading to a transformed earth that is turned 'inside out' with the outer space at the origin and the solid earth at the outside. The Euclidean distances in the new geometry represent the correlations in ozone. The graphics surrounding the sphere show selected correlations based on the new geometry (solid lines) as well as the NMC sample correlations to which they are fit (squares). The globe at the right illustrate the horizontal length scales at the equator. The contour lines enclose the areas that are correlated with the centre.

at middle right of the Fig. 3). In the longitudinal direction, the ozone concentrations become more or less uncorrelated at distances over about 1,500 km in the troposphere, and over 5,000 km in the stratosphere. In the latitudinal direction, the length scale of the correlation is about one third of the longitudinal length scale.

(3) Matrix formulation

For the covariance model in matrix form, we introduce the vector σ and matrix \mathbf{C} for the evaluations of the standard deviation field σ and the above described correlation model C on the grid. The covariance matrix is then formed by:

$$\mathbf{P}[k] = \mathcal{D}(\sigma[k]) \mathbf{C} \mathcal{D}(\sigma[k]). \quad (10)$$

where the matrix $\mathcal{D}(\boldsymbol{\sigma})$ denotes a diagonal matrix with the elements of $\boldsymbol{\sigma}$ on the main diagonal.

5. KALMAN FILTER - FORECAST EQUATIONS

As described in section 2, the first step in the Kalman filter is to compute forecasts for mean and covariance given previous computed entities. According to the Kalman filter equations, the best forecast of the mean state $\bar{\mathbf{x}}$ at a future time is a propagation of the original mean $\bar{\mathbf{x}}^a$ by the model M :

$$\bar{\mathbf{x}}^f_{[k]} = M(\bar{\mathbf{x}}^a_{[k-1]}). \quad (11)$$

The covariance between the true state and this new mean is given by:

$$\mathbf{P}^f_{[k]} = M \mathbf{P}^a_{[k-1]} M^T + \mathbf{Q}_{[k-1]}, \quad (12)$$

where $\mathbf{P}^a_{[k-1]}$ is the covariance of the true state around $\bar{\mathbf{x}}^a$ at time t_{k-1} . With covariance model (10), this becomes:

$$\mathbf{P}^f_{[k]} = (M \mathcal{D}(\boldsymbol{\sigma}^a_{[k-1]})) \mathbf{C} (M \mathcal{D}(\boldsymbol{\sigma}^a_{[k-1]}))^T + \mathbf{Q}_{[k-1]}. \quad (13)$$

There are two problems associated with this propagation. First, the original covariance model (10) is not preserved due to the adding of \mathbf{Q} , and will lead to a full matrix \mathbf{P} which is too large to handle. Second, the model operator M has to be applied once for each column of the diagonal matrix $\mathcal{D}(\boldsymbol{\sigma}^a)$, each representing a field that is zero everywhere except for one point where it has the value of a standard deviation. For a model with only advection, this is the same as advection of the standard deviation field, based on the idea that an error in the estimation of the ozone field is probably unchanged when transported downwind. However, for our model also errors due to uncertainty in the parameterised ozone chemistry should be taken into account.

To avoid both problems, we replace the Kalman covariance propagation (13) by a new, two step process. The first step gives the propagation of the standard deviation field by the advection operator of the model:

$$\boldsymbol{\sigma}^f_{adv[k]} = M_{adv} \boldsymbol{\sigma}^a_{[k-1]}. \quad (14)$$

The second step describes the temporal growth of the standard deviation due to uncertainties in chemistry and meteorological input. It is modelled in a similar manner as the error growth in the total ozone column assimilation (Eskes *et al.* 2003). The growth is applied on the two-dimensional standard deviation field $\boldsymbol{\sigma}_{adv,tot}$ of the total ozone column:

$$(\boldsymbol{\sigma}^f_{tot[k]})^3 = (\boldsymbol{\sigma}^f_{adv,tot[k]})^3 + c \cdot (t_k - t_{k-1}). \quad (15)$$

The relative growth of the total column field from $\boldsymbol{\sigma}^f_{adv,tot}$ to $\boldsymbol{\sigma}^f_{tot}$ is then applied to each individual layer of the three-dimensional field $\boldsymbol{\sigma}^f_{adv}$. The constant c depends on the season and the latitude.

6. GOME OZONE PROFILES

The GOME instrument on board of the ERS2 satellite measures the sunlight backscattered by the atmosphere (Burrows *et al.* 1999). The satellite is placed in a sun-synchronous orbit over the poles. A global coverage is reached within 3 days.

(a) *Profile product*

Ozone profiles are derived from the radiance spectra measured by GOME using the OPERA (Ozone Profile Retrieval Algorithm) retrieval code (Van Oss *et al.* 2002). The algorithm is applied to spectra integrated over 12 sec. time intervals, leading to pixels with a size of approximately 960×100 km. A set of retrieved profiles is available for the year 2000; for computational reasons, profiles have only been calculated for one third of the observations (about 60-70 profiles for each single satellite track).

For each single pixel, the OPERA profile product consists of:

- n_t true levels, defined between $n_t + 1$ pressure levels;
- n_r retrieval levels, defined between $n_r + 1$ pressure levels;
- \mathbf{y}^{ta} : true a-priori profile (n_t);
- \mathbf{y}^{ra} : retrieved a-priori profile (n_r);
- \mathbf{A} : averaging kernel matrix ($n_r \times n_t$);
- \mathbf{S} : error covariance matrix ($n_r \times n_r$);
- \mathbf{y}^r : retrieved profile (n_r).

We now introduce the *true* profile \mathbf{y}^t , as the true, area averaged, vertically discretized profile. The true profile is defined on the true layers specified in the profile product. Each of the points in the true profile is the average ozone concentration in a slab of air between two pressure levels. The true profile is related to the *retrieved* profile \mathbf{y}^r by the averaging kernel (Rodgers 2000):

$$\mathbf{y}^r = \mathbf{y}^{ra} + \mathbf{A} (\mathbf{y}^t - \mathbf{y}^{ta}) + \boldsymbol{\epsilon}, \quad \boldsymbol{\epsilon} \sim \mathcal{N}(\mathbf{0}, \mathbf{S}). \quad (16)$$

The true and retrieved profiles are not necessarily the same. GOME is for example not sensitive to rapid variations in the vertical, and a retrieved profile will therefore not represent these variations but rather a smoothed distribution. The smoothing is described by the averaging kernel matrix \mathbf{A} . The number of significant singular values of the kernel is often much lower than the number of points in the true profile, and the multiplication with \mathbf{A} therefore removes the high frequencies. Some parts of the kernel may be equal or close to zero, indicating that the instrument is not sensitive at certain levels; in that case, the retrieved profile is equal to the a-priori profile. The a-priori profiles are first guesses of the true and retrieved profiles. For OPERA, they are set to the Fortuin-Kelder climatology (Fortuin and Kelder 1998). A-priori profiles serve as reference profiles for linearisations; the retrieval algorithm assumes that the true profile is not too different from the a-priori. The OPERA profiles are defined on the same $n_r = n_t = 40$ layers, such that in the profile product $\mathbf{y}^{ra} = \mathbf{y}^{ta}$. The reason for distinguishing a retrieved a-priori from a true a-priori profile is to account for the possibility that the retrieved product is transformed, as will be done in section 7.

(b) *Comparison with ozone sondes*

To obtain insight in the quality of the GOME profiles, the retrieved profiles are compared with ozone sonde measurements. For the year 2000, a set of more than two-thousand ozone sondes is available from the WOUDC (World Ozone and UV Data Centre) archive. The stations from which the sondes are launched are distributed globally, with the majority located at mid latitudes in the northern hemisphere (Fig. 4). A sonde should have reached the 10 hPa level to be accepted. For each available sonde, we collected all GOME profiles retrieved for the day of sonde launch within 500 km from the launch site. A sonde profile can only be meaningfully compared with GOME profiles if it is convolved with the correct averaging kernel. Hence, a 'true' sonde profile is formed

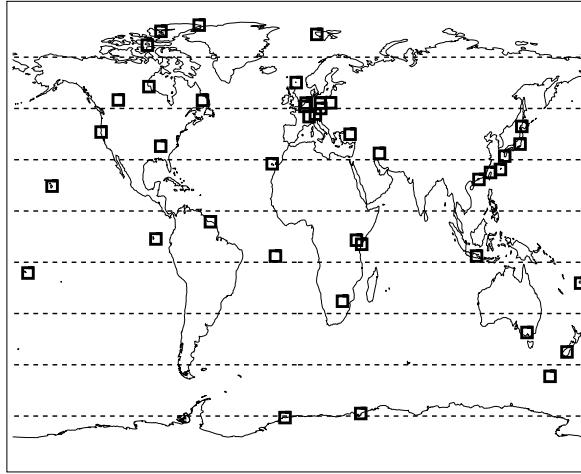


Figure 4. Locations of sonde stations used for validation. The stations are grouped in zonal bands of 20 degrees width.

by averaging the measurements over the pressure layers defined for true profiles, and extension of the profile to the model top by a scaled a-priori profile. A set of 'retrieval' sonde profiles is formed by convolution of the 'true' sonde profiles with the averaging kernels of the selected pixels as in Eq. (16).

Figure 5 shows the bias and standard deviation of the difference between GOME profiles and ozone sondes, as a function of latitude, pressure, and season. The figure shows that strong biases exist in two regions. In the tropical troposphere, a structurally large positive bias of about 2 mPa (about 100%) ozone partial pressure is found. This is of the same order as the standard deviation and therefore not negligible. The inaccuracy of the tropospheric ozone column is not unexpected, since nadir viewing instruments such as GOME are less sensitive for information from altitudes below the ozone maximum. For our study this bias is not dramatic since the focus is on providing high quality stratospheric ozone fields. The second large difference between retrieved profiles and sondes is found in the polar regions during winter conditions. Retrieval of ozone profiles is more difficult here due to the larger solar zenith angles. With a large solar zenith angle, the pathway of solar radiation travelling through the atmosphere to the instrument is much longer, such that only a small amount of the radiation actually reaches the instrument. Only a small number of retrieved GOME profiles is available for large solar zenith angles, and those differ largely from the sondes (right side of upper panels and left side of lowest panels). Furthermore, the extremely low ozone concentrations in the Antarctic winter are not completely captured by the a-priori profiles used in the retrieval, leading to relative large errors too. The standard deviation between retrieved GOME and sonde profiles is rather constant with location and season: around 2 mPa partial pressure, as seen in the right panels. A large part of this spread can be explained from collocation and representation errors between sondes and satellite profiles.

The comparison with sondes indicates that the basic assumptions about the error in the GOME profiles made in (16) are not always completely valid. If we regard the sondes as the 'truth' (they are at least closer to the true state than the satellite profiles), then the difference between the GOME profiles and the true profiles is not unbiased.

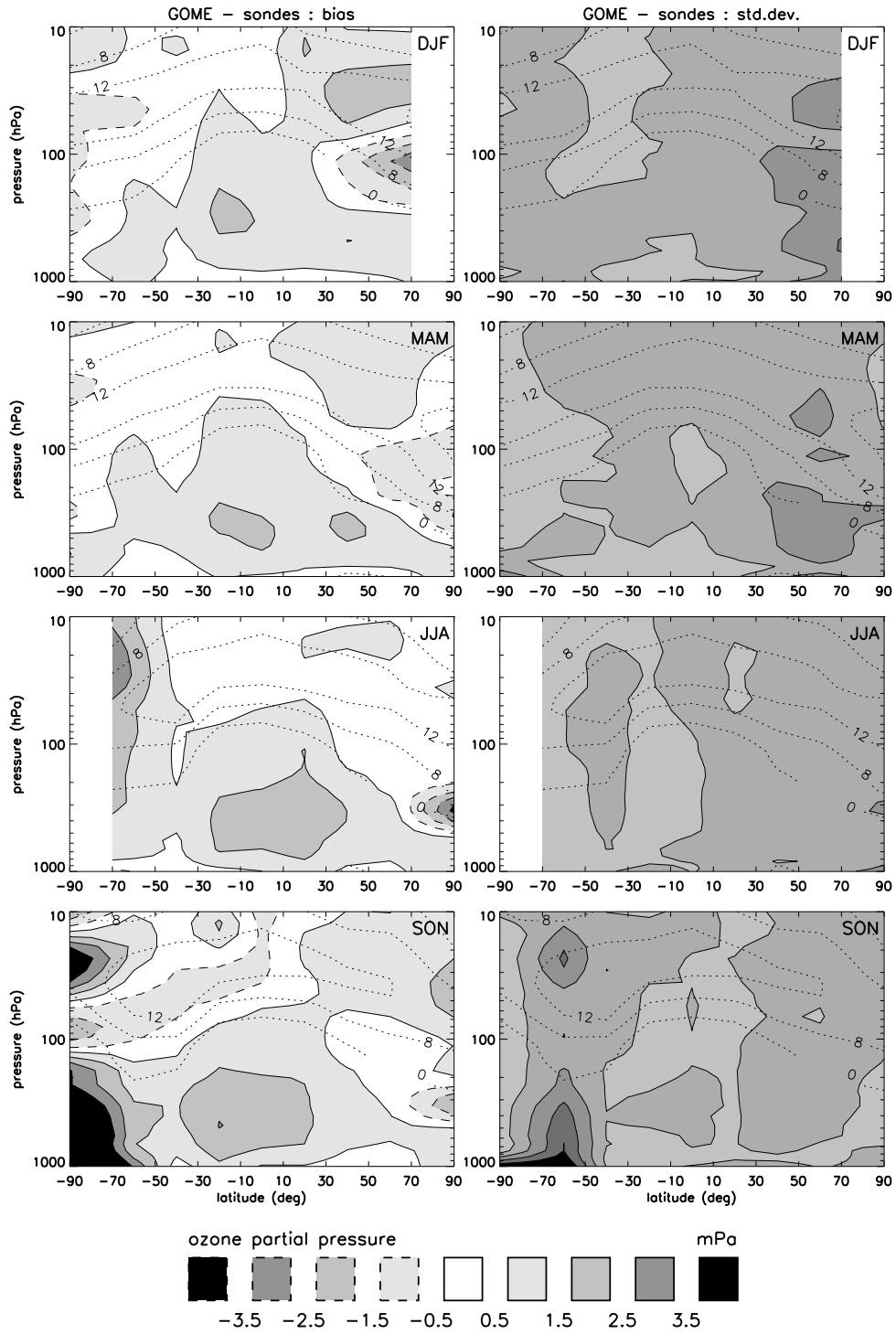


Figure 5. Bias and standard deviation between retrieved GOME ozone profiles and sonde measurements convolved with the averaging kernels, as a function of latitude and season. Pairs of sondes and satellite profiles are collected in latitude bands of 20 degrees; if less than 10 pairs are available, no data is plotted. The dotted lines show the contours of the average ozone partial pressure according to the convolved ozone sondes.

Besides, the difference is larger than what can be expected from the error covariance \mathbf{S} in the profile product. The covariance \mathbf{S} describes the errors due to uncertainties in the measured radiances and in the retrieval algorithm, but not the representation errors. For the assimilation scheme we need a proper description of the measurement error however, preferably unbiased, and with a representative covariance error. A possible way to obtain this is to subtract the observed bias from the retrieved profiles, and to replace the error covariance \mathbf{S} in the profile product by the remaining observed covariance. This method would require a lot of sonde measurements to provide a representative \mathbf{S} , and detailed investigation of why certain sonde measurements differ from the GOME profiles and whether this is persistent or not. Such an investigation is beyond the scope of this study, and therefore left for future improvements of the retrieval algorithm. Instead, a simple but effective algorithm is applied. The bias is simply regarded as a part of the total error, and the error covariance \mathbf{S} in the profile product is replaced by values representative for the total error. A large error is therefore accepted where the GOME profiles are strongly biased compared to the sondes, and as a result, the information in these profiles will hardly be used in the assimilation.

A new error covariance matrix \mathbf{R} is formed to replace \mathbf{S} , by scaling the rows and columns of \mathbf{S} such that the new standard deviations are equal to the RMS (root-mean-square) errors between GOME profiles and sondes. The RMS error can be interpreted as the sampled standard deviation of the error ϵ in (16). RMS values are obtained on a latitude/pressure/season grid in the same way as the bias and standard deviations of Fig. 5. The cross-correlations in \mathbf{R} are the same as in the original \mathbf{S} provided by the retrieval. An estimate of the cross-correlations could be extracted from the observed GOME-sonde differences too, but the number of sondes is too limited to obtain these with the desired accuracy.

7. OBSERVATION OPERATOR

With both the model state and the measurements defined, it is now possible to define an observation operator. The observation operator should simulate a retrieved GOME ozone profile given the model state \mathbf{x} following (2b). Eq. (16) describes what is retrieved from GOME if it observes the true profile \mathbf{y}^f . Therefore, a simple method to build an observation operator is to set \mathbf{y}^t to the profile described by the model state:

$$\mathbf{y}^t = \mathbf{B} \mathbf{G} \mathbf{x}. \quad (17)$$

Operator \mathbf{G} denotes a horizontal interpolation of the TM3 profiles. The result is a single profile defined at the vertical model levels. For convenience, the horizontal interpolation is a simple bi-linear interpolation from the surrounding grid cells to the centre of the satellite footprint. This method suffers slightly from the fact that the GOME footprints are rather broad (about 960×100 km). However, involving much more TM3 grid cells in the horizontal interpolation than the 4 that are surrounding the footprint centre would significantly increase the computational demand for the calculation of correlations between a GOME profile and other profiles. Operator \mathbf{B} denotes vertical projection from the TM3 model layers to the n_t true layers of the GOME profile.

To form an observation operator following (2b), convolution (16) is applied to (17):

$$H(\mathbf{x}) = \underbrace{\mathbf{y}^{ra} - \mathbf{A}\mathbf{y}^{ta}}_{H_0} + \underbrace{\mathbf{A}\mathbf{B}\mathbf{G}}_{\mathbf{H}} \mathbf{x} + \mathbf{v}, \quad \mathbf{v} \sim \mathcal{N}(\mathbf{o}, \mathbf{R}). \quad (18)$$

The observation error covariance \mathbf{R} is therefore set to the scaled retrieval error covariance \mathbf{S}^n obtained from the comparison between retrieved GOME profiles and sondes as

described in the previous section. We assume that the representation error between the model profile computed with the **BG** operator and the GOME profiles is comparable with the representation error between sondes and GOME profiles.

The number of data elements in $H(\mathbf{x})$ is much larger (about 40) than the actual degree of freedom in the retrieved product (about 5). The large amount of data points is undesired, since the costs of some analysis operations in the Kalman filter grow quadratically with the number of data elements. To limit the number of data points, the retrieved profile should be reduced to a smaller vector without losing information. An appropriate method to do this is via the averaging kernel matrix \mathbf{A} . Equation (16) shows that retrieved profiles are computed as a linear combination of the columns of \mathbf{A} . Since the singular values of \mathbf{A} quickly decay to zero, the retrieved profiles can be approximated by a linear combination of a limited number of well chosen vectors. The left singular vectors of \mathbf{A} are an appropriate choice. Let $\mathbf{A} \approx \mathbf{U}\mathbf{\Sigma}\mathbf{V}^T$ be the singular value decomposition of \mathbf{A} , truncated at a number of singular vectors equal to the actual degrees of freedom of the profile (part of the profile product). A transformed retrieved profile is formed by $\tilde{\mathbf{y}}^r = \mathbf{U}^T \mathbf{y}^r$ which has a number of elements equal to the degree of freedom. The elements represent coefficients in a space spanned by the columns of \mathbf{U} . The corresponding observation operator \tilde{H} is similar to (18):

$$\tilde{H}(\mathbf{x}) = \tilde{\mathbf{y}}^{ra} - \tilde{\mathbf{A}}\mathbf{y}^{ta} + \tilde{\mathbf{A}}\mathbf{B}\mathbf{G}\mathbf{x} + \tilde{\mathbf{v}}, \quad \tilde{\mathbf{v}} \sim \mathcal{N}(\mathbf{0}, \tilde{\mathbf{R}}). \quad (19)$$

where $\tilde{\mathbf{y}}^{ra} = \mathbf{U}^T \mathbf{y}^{ra}$, $\tilde{\mathbf{A}} = \mathbf{\Sigma}\mathbf{V}^T$, $\tilde{\mathbf{v}} = \mathbf{U}^T \mathbf{v}$, and $\tilde{\mathbf{R}} = \mathbf{U}^T \mathbf{R}\mathbf{U}$.

8. KALMAN FILTER - ANALYSIS EQUATIONS

Whenever measurements are available, the forecasts of mean and covariance defined in section 5 are replaced by an analysis incorporating the new information. In this study, all profiles retrieved during a single orbit of GOME are collected into a track, which is treated as a single measurement, valid for a mean time. A track contains profiles that are retrieved for solar zenith angles less than 75 degrees. The reason for not analysing the retrieved profiles one by one is twofold. First, the computational costs would be much larger, since analysing profiles one by one would imply an update of the state elements for each profile again instead of only once. Second, the analysis equations will be applied to the variance field only to maintain the chosen covariance parameterisation, which introduces a small error in comparison with an analysis applied to a full covariance matrix; analysing the profiles one by one will lead to accumulation of this error. It is therefore common practise to analyse a large amount of measurements together at once, although they are strictly speaking not all observed at exactly the same time. For convenience, the notations $\tilde{\mathbf{y}}$, $\tilde{\mathbf{H}}$, $\tilde{\mathbf{R}}$ etc. will be used from now on to describe entities that refer to a complete track, instead of just a single profile.

The first step in the analysis stage of the Kalman filter is the analysis of the mean state using a linear gain:

$$\bar{\mathbf{x}}^a = \bar{\mathbf{x}}^f + \mathbf{K} (\tilde{\mathbf{y}}^r - \tilde{H}(\bar{\mathbf{x}}^f)). \quad (20)$$

The forecast of the mean is adapted relative to the difference between the retrieved track $\tilde{\mathbf{y}}^r$ and the simulated track $\tilde{H}(\bar{\mathbf{x}}^f)$. The gain matrix \mathbf{K} acts as a point-spread function, distributing the update toward the retrieved track over the elements of the state. For the gain we use the common used Kalman gain:

$$\mathbf{K} = \mathbf{P}^f \tilde{\mathbf{H}}^T (\tilde{\mathbf{H}}\mathbf{P}^f \tilde{\mathbf{H}}^T + \tilde{\mathbf{R}})^{-1}. \quad (21)$$

The second step in the analysis is to compute the covariance of the true state around the analysed mean:

$$\mathbf{P}^a = (\mathbf{I} - \mathbf{K}\tilde{\mathbf{H}})\mathbf{P}^f(\mathbf{I} - \mathbf{K}\tilde{\mathbf{H}})^T + \mathbf{K}\tilde{\mathbf{R}}\mathbf{K}^T \quad (22)$$

where \mathbf{I} denotes the identity matrix. In our covariance model defined in Eq. (10), operations are to be performed on the standard deviation field, while the correlation function is constant. It is therefore sufficient to compute the impact of (22) on the variance field only:

$$(\boldsymbol{\sigma}^a)^2 = \text{diag} \left((\mathbf{I} - \mathbf{K}\tilde{\mathbf{H}})\mathbf{P}^f(\mathbf{I} - \mathbf{K}\tilde{\mathbf{H}})^T + \mathbf{K}\tilde{\mathbf{R}}\mathbf{K}^T \right) \quad (23a)$$

$$= \text{diag} \left(\mathbf{P}^f \right) - 2 \text{diag} \left(\mathbf{K}\tilde{\mathbf{H}}\mathbf{P}^f \right) + \text{diag} \left(\mathbf{K}[\tilde{\mathbf{H}}\mathbf{P}^f\tilde{\mathbf{H}}^T + \tilde{\mathbf{R}}]\mathbf{K}^T \right). \quad (23b)$$

The Kalman gain Eq. (21) is regarded as *statistically optimal* since it minimises the variance described by (22). Matrix \mathbf{K} can be solved from the matrix-matrix equation implied by (21). A complication is that the matrix $\tilde{\mathbf{H}}\mathbf{P}^f\tilde{\mathbf{H}}^T + \tilde{\mathbf{R}}$ is badly conditioned. Due to the strong spatial correlations between the pixels in a track, the eigenvalue spectrum of the matrix consists of only a few large eigenvalues and many smaller ones. To make the matrix better conditioned one could choose to add a diagonal matrix to $\tilde{\mathbf{R}}$. This is equivalent to assigning extra representation errors to all elements of $\tilde{\mathbf{y}}$, that are not correlated with any other element. Unfortunately, a good choice for such an extra representation error for $\tilde{\mathbf{y}}$ is hard to make, since the associated representation error for \mathbf{y} (that follows from the backward transformation with singular vectors of the averaging kernel) is rather unrealistic.

To overcome these problems, the measurements are projected on a subset of the eigenvectors of $\tilde{\mathbf{H}}\mathbf{P}^f\tilde{\mathbf{H}}^T + \tilde{\mathbf{R}}$. Computation of the largest eigenvalues is relatively cheap using standard linear algebra libraries. The matrix is approximated by an eigenvalue decomposition, truncated at a number of eigenvalues (about 30-50%) representing 98% of the original trace (empirical choice):

$$\tilde{\mathbf{H}}\mathbf{P}^f\tilde{\mathbf{H}}^T + \tilde{\mathbf{R}} \approx \hat{\mathbf{E}}\hat{\boldsymbol{\Lambda}}\hat{\mathbf{E}}^T. \quad (24)$$

After this reduction, the 'condition' number (largest eigenvalue divided by smallest non-zero eigenvalue) is of the order 10^2 . The original model state projection (19) is now replaced by:

$$\hat{H}(\mathbf{x}) = \hat{\mathbf{E}}^T(\tilde{\mathbf{y}}^{ra} - \tilde{\mathbf{A}}\mathbf{y}^{ta}) + \hat{\mathbf{H}}\mathbf{x} + \hat{\mathbf{v}}, \quad \hat{\mathbf{v}} \sim \mathcal{N}(\mathbf{o}, \hat{\mathbf{R}}). \quad (25)$$

where $\hat{\mathbf{y}} = \hat{\mathbf{E}}^T\tilde{\mathbf{y}}$, $\hat{\mathbf{H}} = \hat{\mathbf{E}}^T\tilde{\mathbf{H}}^T$, and $\hat{\mathbf{R}} = \hat{\mathbf{E}}^T\tilde{\mathbf{R}}\hat{\mathbf{E}}$. The gain matrix can then be solved from the simple diagonal equation

$$\hat{\boldsymbol{\Lambda}}\hat{\mathbf{K}}^T = \hat{\mathbf{H}}\mathbf{P}^f \quad (26)$$

and the analysis equations become:

$$\bar{\mathbf{x}}^a = \bar{\mathbf{x}}^f + \hat{\mathbf{K}}(\hat{\mathbf{y}}^r - \hat{H}(\bar{\mathbf{x}}^f)) \quad (27a)$$

$$(\boldsymbol{\sigma}^a)^2 = (\boldsymbol{\sigma}^f)^2 - 2 \text{diag} \left(\hat{\mathbf{K}}\hat{\mathbf{H}}\mathbf{P}^f \right) + \text{diag} \left(\hat{\mathbf{K}}\hat{\boldsymbol{\Lambda}}\hat{\mathbf{K}}^T \right). \quad (27b)$$

9. ASSIMILATION RESULTS

The one year data set of GOME ozone profiles available for the year 2000 (see section 6) is assimilated with the above described assimilation system. The assimilation is initialised with a 3D ozone and standard deviation field taken from a total ozone assimilation.

(a) *Internal consistency*

An important test for the quality of an assimilation is whether the differences between model forecast and observations satisfy the assumed statistics. The assumed statistics can be summarised in the requirement that the actual innovations (differences between observation and their model forecast) have a Gaussian distribution (Ménard and Chang 2000):

$$\mathbf{y} - \mathbf{H}\bar{\mathbf{x}}^f \sim \mathcal{N}(\mathbf{o}, \mathbf{H}\mathbf{P}^f\mathbf{H}^T + \mathbf{R}). \quad (28)$$

The zero mean and covariance $\mathbf{H}\mathbf{P}^f\mathbf{H}^T + \mathbf{R}$ at the right hand side follow directly from the assumptions about the true state and the observations (distributed around the mean state and observations with zero mean and covariance \mathbf{P}^f and \mathbf{R} respectively). That the observed innovations match with the assumed statistics is a minimum requirement for having a consistent covariance model.

Figure 6 shows an example of the average bias between observations and model forecasts, obtained for the months of March-May. In here, the observations consist of the GOME retrieved ozone profiles in their native form (without any projection on modes that is required for solving the analysis equations); the model forecast is the corresponding TM3 ozone profile after convolution with the averaging kernels. The figure shows that the bias oscillates around zero with respect to altitude. The absolute amplitude of the fluctuation is about 0.5 mPa in ozone partial pressure, which is small with respect to the spread (shaded area in figure) in most of the atmosphere. The smallest bias is found for the lower and middle stratosphere, roughly from tropopause to about 8 hPa. The ozone maximum in the assimilation product is therefore on average in good agreement with the GOME profiles. Relative large biases are found for the troposphere and above 8 hPa. For the troposphere this is no surprise, since a large representation error is assigned to the GOME profiles here as a result of the validation with sondes from section 6(b). Tropospheric information from the GOME profiles is therefore hardly used in the assimilation. At the top of the atmosphere, the relative strong fluctuation in bias and small spread indicates a persistent difference between the model and the GOME profiles. A possible explanation is that the chemistry timescale is rather short at these altitudes, and the assimilation of measurements only once per day is unable to remove a bias between model and observations. Another possible explanation is that the climatology used for the parameterised ozone chemistry slightly differs from the a-priori profiles in the retrieval, or is not exactly valid at the overpass time of GOME. The impact of the use of climatologies at different stages of the total assimilation system is subject of further study. The best approach to avoid the use of different climatologies is to directly assimilate the radiances measured by GOME. The retrieval step from radiance spectra to retrieved profiles is then replaced by an incorporation of the forward radiative transfer model in the observation operator. This requires detailed knowledge of the instrument and the measured spectra however, and this expertise is not easily embedded in an assimilation system. For the future, assimilation of radiances is however an interesting option.

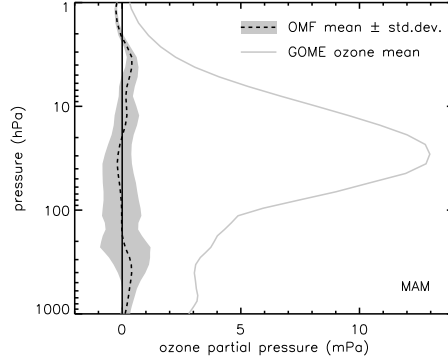


Figure 6. Observation-minus-forecast mean \pm std.dev. for the retrieved (including kernels) GOME ozone profiles during assimilation. Taken over all available profiles for March-May 2000. The solid line shows the mean retrieved profile.

A small bias between forecast and observation is acceptable if it is not too large in comparison with the uncertainty assigned to the forecast and the observation. A simple check to judge whether this is true is to apply (28) for all individual measurements i by computing the ratio between observed residue and forecasted standard deviation, which should have a standard normal distribution:

$$\frac{\text{omf}}{\sigma(\text{omf})} = \frac{y_i - \mathbf{h}_i^T \mathbf{x}^f}{\sqrt{\mathbf{h}_i^T \mathbf{P}^f \mathbf{h}_i + r_{ii}}} \sim \mathcal{N}(0, 1) \quad (29)$$

where \mathbf{h}_i^T is a row of \mathbf{H} and r_{ii} a diagonal element of \mathbf{R} . Figure 7 shows histograms of the computed ratio's for altitudes below 300 hPa ('lower troposphere'), between 300 and 10 hPa ('ozone layer / UTLS (upper troposphere/lower stratosphere)'), and above 10 hPa ('upper stratosphere'). In the region of ozone layer/UTLS, the sample distribution of the ratio is close to the expected standard normal distribution. The OMF samples are perfectly unbiased, indicating that the assimilation is doing a good job at these altitudes. The number of realisations with a large ratio is only a little larger than what it should be. This indicates a small under estimation of the observation-minus-forecast standard deviation, which is not unusual in assimilations (Ménard and Chang 2000). For the bottom and top of the atmosphere, clear biases are left. In the lower troposphere, more than 90% of the observation-minus-forecast realisations is positive. This bias is related to the large overestimation of the ozone values in the tropical troposphere, as seen in Fig. 5. To account for this bias, a relative large representation error covariance is assigned to the observations (r_{ii} in Eq. (29)). This is visible in Fig. 7 by the fact that the sample probability density for the troposphere is peaked or less broad than a standard normal distribution, related to the large denominators in the $\text{omf}/\sigma(\text{omf})$ ratios. In the upper stratosphere, two peaks are visible in the probability density, caused by an oscillation in observation-minus-forecast with respect to altitude as seen in Fig. 6. The density is also rather broad. Above 10 hPa, no sonde data is used to assign a representation error covariance to the observations, and the chosen a-priori value under estimates the true representation error. The expected standard deviation of observation-minus-forecast is therefore under estimated, and this leads to large ratio's in Eq. (29) for the upper stratosphere.

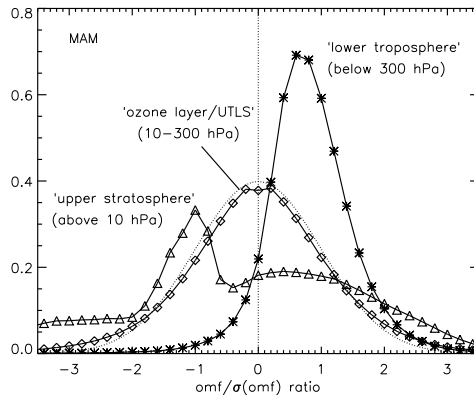


Figure 7. Sample probability density functions of ratio between actual observation-minus-forecast and the expected standard deviation. The samples are taken over March-May 2000 and three vertical regions. The theoretical distribution is a standard normal one, which is plotted as a dashed line.

(b) *Comparison with GOME total ozone retrievals*

Figure 8(a) shows the distribution of observation-minus-forecast of total ozone, as a function of latitude. The OPERA ozone profiles are summed to a total column, and compared with the model forecast just before assimilation. The shaded area in the figure shows the bias and the spread in the differences. The bias is in general small: 5-10 DU while the standard deviation is in the order of 10-20 DU. The only exception is the tropics, where the OPERA total columns on average exceed the model forecasts due to the overestimation of the tropospheric profile (see section 6(b)). Figure 8(b) shows the forecast bias in total ozone for two other GOME products: KNMI's NRT (Near Real Time) product (Valks *et al.* 2003) and the ESA GDP3 (GOME Data Processor) (Spurr *et al.* 2002) product. Although all products are based on measurements from the same instrument, the total ozone estimates differ from each other due to differences in the retrieval algorithms. The NRT product is known to have a negative bias for large solar zenith angles, which is visible in the OMF statistics. The GDP product is extensively validated in (Lambert *et al.* 2002). The OPERA total column is systematically larger than the other total columns. As can be expected from the fact that the OPERA profiles are assimilated, both the bias as well as the spread are the smallest for this set.

(c) *Validation with ozone sondes*

The assimilated ozone fields are compared with the ozone sondes described in section 6(b). For this, the ozone profile above the launch site of a sonde is extracted from the analysis. Figure 9 shows the bias and standard deviation between sondes and assimilation, as a function of latitude and season. In this comparison, neither the sondes nor the model simulations are convolved by averaging kernels. This is the best way to judge the quality of the analysed fields, since it is a direct comparison with high resolution independent data. However, it is difficult to relate observed biases between analysis and sondes to biases between GOME and sondes as shown in Fig. 5, since the later is based on convolved profiles. To illustrate the effect of the convolution with averaging kernels, three different validations with sondes are plotted in Fig. 10.

The results in Fig. 9 show that the relatively smallest biases between analysed fields and ozone sondes are found around the ozone layer (except for the polar regions). The absolute bias is here in general less than 0.5 mPa ozone partial pressure, which is about

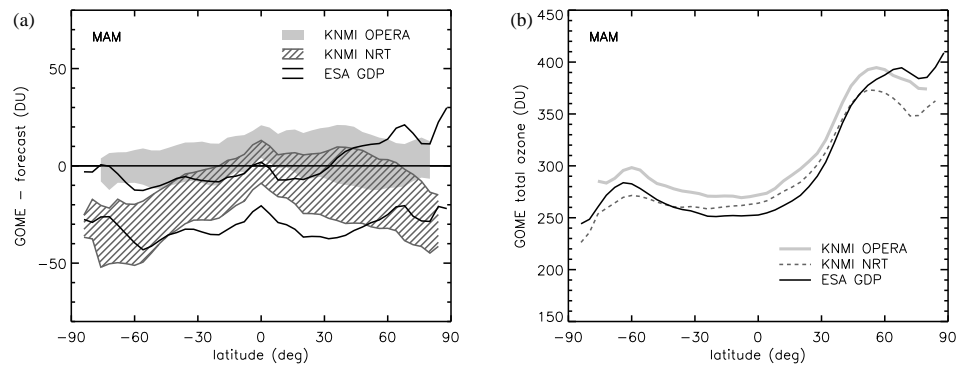


Figure 8. (a) 'Observed GOME total ozone' minus 'TM3 total ozone forecast' over March-May 2000, for different GOME total ozone data sets. The enclosed areas represent the mean plus/minus standard deviation. (b) mean observed GOME total ozone for same period.

4% of the ozone concentration and which is small in comparison with the standard deviation of 0.5-1.5 mPa (about 10%). In the lower stratosphere (below the ozone layer), both the bias and the standard deviation are somewhat larger: about 0.5-1.5 mPa (10%) and 1.5-2.5 mPa (20%) respectively.

The largest absolute differences between assimilation and sondes occur in the polar regions in winter, especially at the south pole (bottom figures). The number of GOME profiles available for this region and season is limited, and measurement data is therefore hardly incorporated in the assimilation here. Besides, the limited vertical resolution of the GOME profiles hampers the removal of this particular biases. Fig. 10 shows that the strong oscillation in the bias that is found when comparing assimilation with sondes directly (lower left), is not present after convolution with averaging kernels (middle left). The small scale bias is therefore not visible during the assimilation, and can not be corrected for.

Relative large biases in the analysed fields are also found in the tropical troposphere, similar as seen in Fig. 5 for the comparison between GOME and sondes. The assimilated ozone profiles exceed the sonde measurements with 1-2 mPa partial pressure here.

Comparison of the validation results for GOME vs sondes and assimilation vs sondes (upper rows in Fig. 10) shows that the assimilation has an added value over the GOME data especially outside the tropics. At mid latitudes, both the biases and the standard deviations are strongly decreased. In the Arctic region, the large scale oscillation in the bias that is sometimes present in the GOME profiles disappears almost completely after assimilation. The model simulation clearly adds information to the analysis in these regions. In the tropics, the added value is much smaller. Retrieval and model are in agreement with each other here: both overestimate the sonde measurements in more or less the same way. Thus, the GOME profiles hardly have impact on the assimilation here, even if a small representation error covariance is assigned rather than the large value that is assigned in our experiments. The reason for assigning a large error covariance has to do with the large bias observed in the retrieved profiles, and that is not changed by the fact that model and retrieval are biased in the same way.

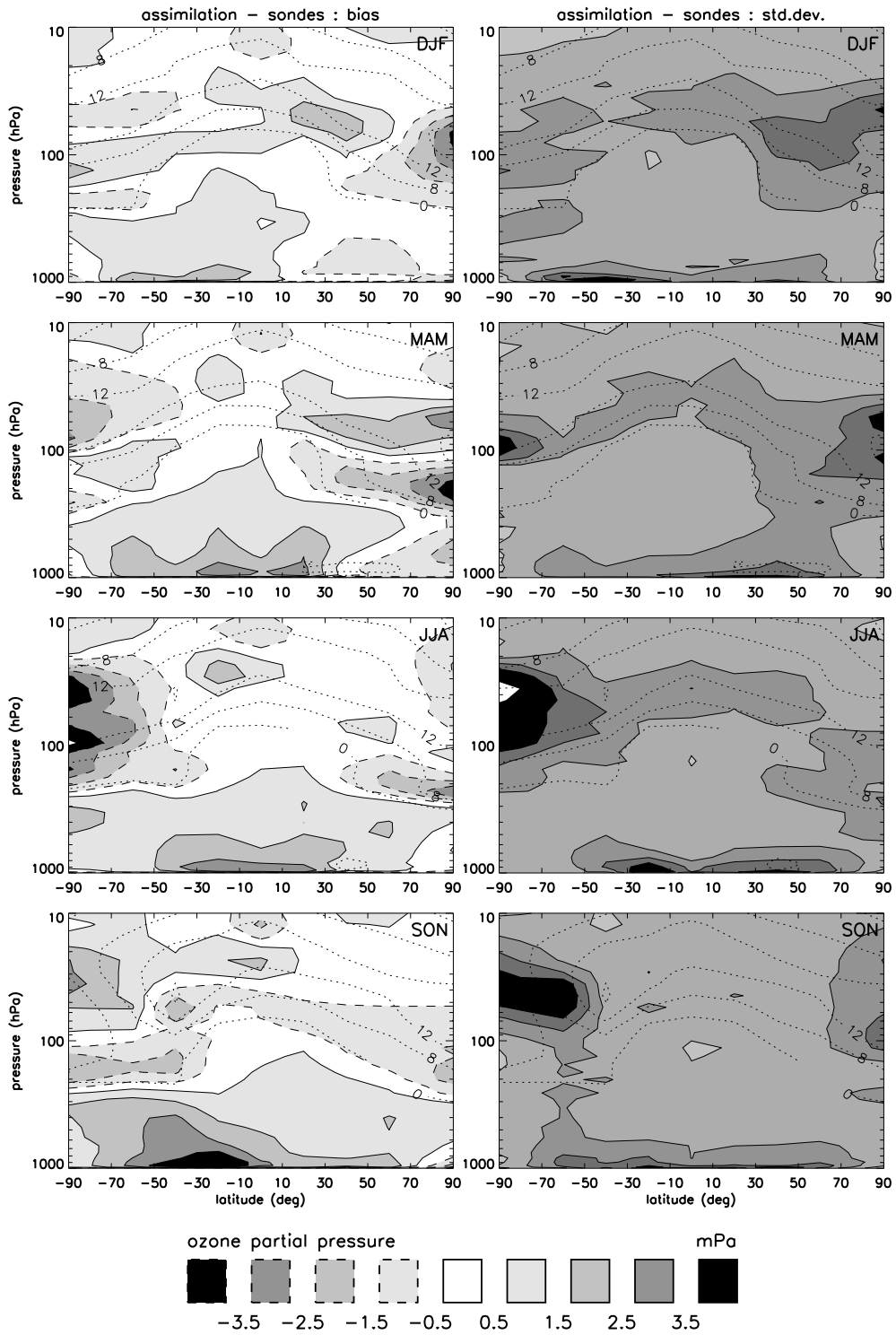


Figure 9. Bias and standard deviation between assimilated fields and ozone sonde measurements as a function of latitude and season. The dotted lines show the average ozone concentration according to the ozone sondes.

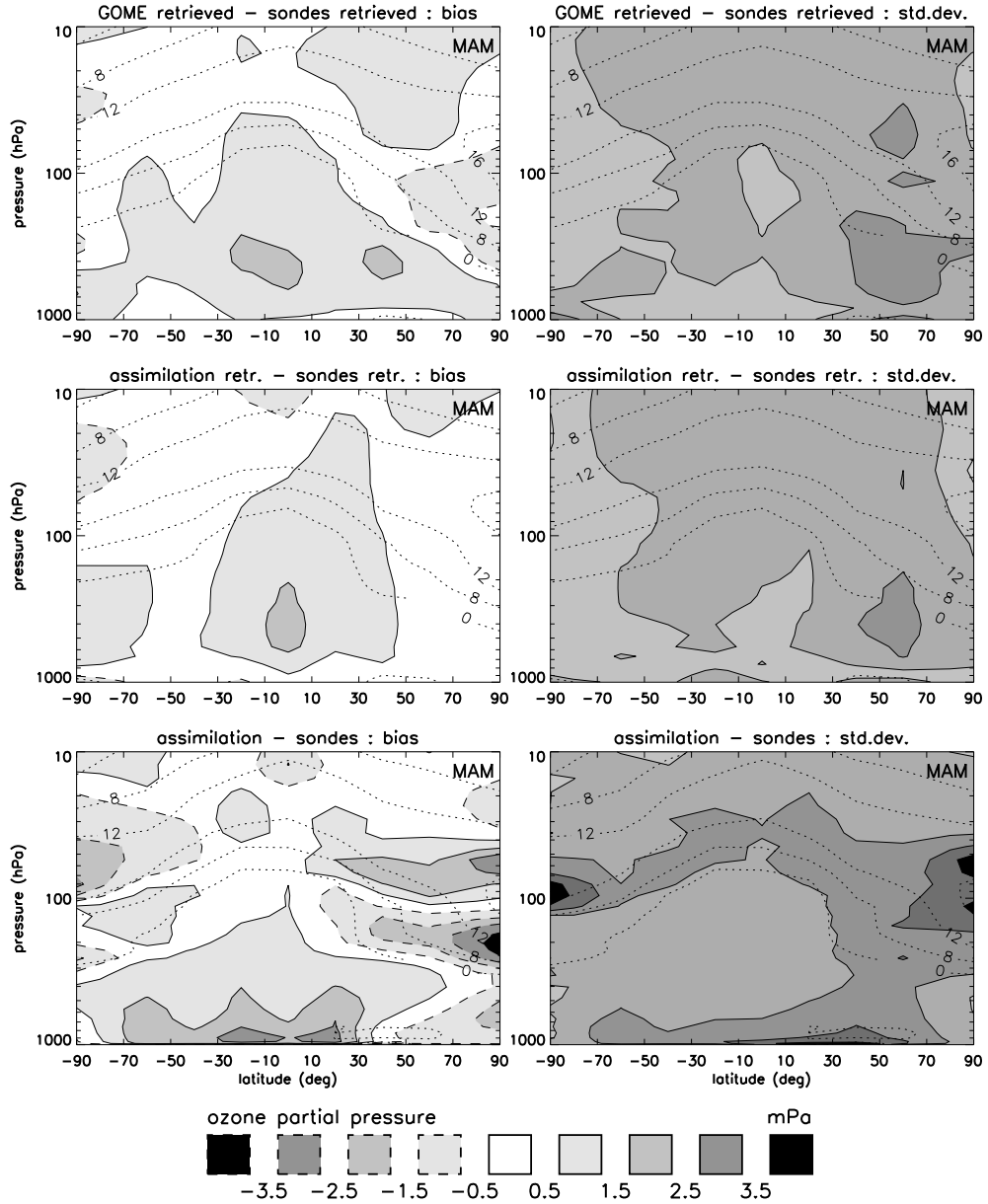


Figure 10. Illustration of difference between validation against 'retrieved' ozone sondes (convolved with averaging kernels) and 'raw' sondes. Top: GOME ozone profiles vs sondes (retrieved); same as Fig. 5. Middle: analysed state interpolated to GOME profiles vs sondes (retrieved). Bottom: analysed state vs sondes (raw); same as Fig. 9.

(d) *Impact of ozone profiles in assimilation: a case study*

In comparison with assimilation of total ozone, the assimilation of ozone profiles is much more expensive due to the larger data volume. For the extra expense on computational resources, we expect at least a better representation of the vertical ozone distribution. To test whether assimilation of ozone profiles adds value to an assimilation of the total column only, a case study is carried out for April 2000. Around 12 April, an intrusion of ozone rich air from the Arctic is visible over Europe (Fig. 11(a)). Sonde measurements show the intrusion as a pronounced secondary maximum in the ozone profile around 150 hPa (Fig. 11(b)).

Starting at 1 April from an analysed initial field from the one-year assimilation run, three TM3 simulation runs are created: 1) without any assimilation; 2) with assimilation of GOME ozone profiles summed to total columns; 3) with assimilation of the GOME ozone profiles. In both assimilation runs, all available pixels are used instead of only one third, which was necessary for the one year run. The assimilation of total columns is implemented by a summation of the rows of the averaging kernels in the profile product, similar as the projection on singular vectors described in section 7. The kernel of the total column is a row vector specifying the sensitivity of the retrieval for ozone at different pressure levels. In the stratosphere it has a value of 1.0, while it decreases to zero toward the troposphere where the instrument is hardly sensitive to ozone.

The vertical structure in the model forecast without assimilation is already close to the profile measured by sondes, as shown for the sonde launched from Payerne in Fig. 11(b). The vertical shape of the ozone profile seems to be well described by the wind and temperature fields of the ECMWF model and simple parameterised ozone chemistry (Eskes *et al.* 2004). The forecast of the total ozone column by the model is already rather good: an under estimation of the top ozone maximum is compensated by a minimum between the two maximums that is over estimated. Assimilation of the total ozone column therefore helps to limit the amplitude of the vertical variations, but does not provide extra information during the intrusion. However, assimilation of ozone profiles leads to an analysed profiles that almost exactly follow the available sonde measurements. The maximums and the minimum are much more pronounced, despite the limited (about 5 km) vertical resolution of the GOME profiles. The only explanation is a structural better simulation of the stratospheric ozone maximum and the Arctic intrusion during the days before the launch of the sondes. Leaving the perturbation of the tropospheric profile for future study, the example suggests that information on strong vertical ozone gradients in middle and lower stratosphere can be obtained from assimilation of ozone profiles retrieved from GOME.

10. CONCLUSIONS

An assimilation system for ozone profiles retrieved from the GOME satellite instrument has been presented. The system is based on the Kalman filter equations and is an extension of a total column assimilation to three dimensions.

A three dimensional anisotropic covariance model has been developed using the NMC method. The model accounts for the different correlation scales in ozone with respect to altitude and longitude. Further fine tuning of the covariance model will be performed during multi-year assimilations. Possible improvements are for example a seasonal dependence, and an error growth that is specially tuned for the new covariance model. Such tuning experiments will be used to study the impact of the anisotropic covariance model in comparison with isotropic models.

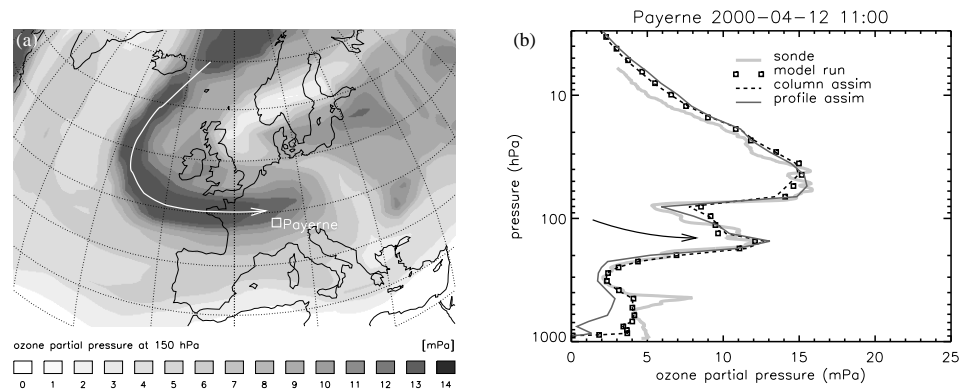


Figure 11. (a) Intrusion of ozone rich air from the Arctic over Europe at a height of 150 hPa, 12 April 2000 1100 UTC. (b) Ozone profiles measured and simulated at Payerne at the same time. Similar profiles are found for sondes launched from Uccle, Hohenpeisenberg, and Prague.

Including the averaging kernels of the GOME profile product in the observation operator is essential for correctly use of the observations during comparison of modelled or measured profiles with the satellite profiles. Beside, the kernels provide an efficient method to reduce the data volume by projection of the measurements on their singular vectors.

The GOME ozone profiles provide useful information on the ozone distribution. After assimilation, an overall error of 1.5-2.5 mPa in ozone partial pressure remains between assimilated ozone and sonde measurements around the ozone maximum. Improvements have to be made in the troposphere and in the polar regions under winter conditions, where a relative large representation error has to be assigned to the GOME profiles. A case study concerning an intrusion of Arctic air over Europe suggests that the assimilation of GOME profiles improves the simulation of the ozone distribution even in the case of strong vertical gradients.

ACKNOWLEDGEMENTS

A.J. Segers has been supported by the project SASCIA of the Space Research Organisation Netherlands (SRON) and Netherlands Organisation for Scientific Research (NWO). H.J. Eskes has been supported by the European Union GOA project (contract no EVK2-CT-2000-00062) and the European Union ASSET project (contract EVK2-CT-2002-00137). We thank the World Ozone and Ultraviolet Radiation Data Centre (WOUDC) and the sonde teams for providing ozone sonde data at <http://www.woudc.org/>. We also thank the two anonymous reviewers for helpful comments.

REFERENCES

- | | | |
|---|------|--|
| Bregman, A., Segers, A., Krol, M., Meijer, E. and Van Velthoven, P. | 2003 | On the use of mass-conserving wind fields in chemistry-transport models. <i>Atmos. Chem. Phys.</i> , 3 , 447–457 |
| Burrows, J. P., Weber, M., Buchwitz, M., Rozanov, V., Ladstätter-Weibenmayer, A., Richter, A., Debeek, K., Eichmann, K. U., Eisinger, M. and Perner, D. | 1999 | The Global Ozone Monitoring Experiment (GOME): Mission concept and first results. <i>J. Atmos. Sci.</i> , 56 , no. 2, 151–175 |

- Cariolle, D. and D'equ'e, M. 1986 Southern hemisphere medium-scale waves and total ozone disturbances in a spectral general circulation model. *J. Geophys. Res.*, **91** 10825–10846
- Dethof, A. and Holm, E. 2002 'Ozone in era40: 1991-1996'. Technical Memorandum 377, ECMWF, Reading, UK.
- EC (European Commission) 2003 'Ozone-climate interactions'. Air pollution research report No 81, 143 pp
- El Serafy, G. Y. and Kelder, H. M. 2003 Near-real-time approach to assimilation of satellite-retrieved 3D ozone fields in a global model using simplified Kalman filter. *Q. J. R. Meteorol. Soc.*, **129**, 3099–3120
- Elbern, H. and Schmidt, H. 2001 Ozone episode analysis by four-dimensional variational chemistry data assimilation. *J. Geophys. Res.*, **106**, no. D4, 3569–3590
- Errera, Q. and Fonteyn, D. 2001 Four dimensional variational chemical assimilation of CRISTA stratospheric measurements. *J. Geophys. Res.*, **106**, no. D11, 12,253–12,265
- Eskes, H. J., Van Velthoven, P. F. J., Valks, P. and Kelder, H. M. 2003 Assimilation of gome total ozone satellite observations in a three-dimensional tracer transport model. *Q. J. R. Meteorol. Soc.*, **129**, 1663
- Eskes, H. J., Segers, A. J. and Van Velthoven, P. F. J. 2004 'Ozone Forecasts of the Stratospheric Polar Vortex Splitting Event in September 2002.' *J. Atmos. Sci.*, special issue on the Antarctic stratospheric sudden warming and split ozone hole of 2002.
- Fierli, F., Hauchecorne, A., Bekki, S., Theodore, B. and d'Andon, O. F. 2002 Data assimilation of stratospheric ozone using a high-resolution transport model. *Geophys. Res. Lett.*, **29**, no. 10, doi:10.1029/2001GL014272
- Fisher, M. and Lary, D. 1995 Lagrangian four-dimensional variational data assimilation of chemical species. *Q. J. R. Meteorol. Soc.*, **121**, no. 7, 1681–1704
- Fortuin, J.P.F. and Kelder, H.M. 1998 An ozone climatology based on ozonesonde and satellite measurements. *J. Geophys. Res.*, **103**, 1517–1520
- Gaspari, G. and Cohn, S. E. 1999 Construction of Correlation Functions in Two and Three Dimensions. *Q. J. R. Meteorol. Soc.*, **125** 723–757
- Hadjinicolaou, P. and Pyle, J.A. 2004 The Impact of Arctic Ozone Depletion on Northern Middle Latitudes: Interannual Variability and Dynamical Control. *J. Atmos. Chem.*, **47**, no. 1, 25–43
- Hasekamp, O. P. and Landgraf, J. 2001 Ozone profile retrieval from backscattered ultraviolet radiances: The inverse problem solved by regularizations. *J. Geophys. Res.*, **106**, 8077–8088
- Hoogen, R., Rozanov, V. V. and Burrows, J. P. 1999 Ozone profiles from GOME satellite data: Algorithm description and first validation. *J. Geophys. Res.*, **104**, 8263–8280
- IPCC 2001 'Climate Change 2001, The Scientific Basis'. Contribution of Working Group 1 to the Third Assessment Report. Houghton, J.T. *et al.* (Eds.), Cambridge Univ Press, Cambridge, UK, 881 pp
- Khattatov, B., Lamarque, J.-F., Lyjak, L., Menard, R., Levelt, P., Tie, X., Brasseur, G., and Gille, J. 2000 Assimilation of satellite observations of long-lived chemical species in global chemistry transport models. *J. Geophys. Res.*, **105**, no. D23, 29135–29144
- Lambert, J.-C. (editor) 2002 'ERS-2 GOME GDP 3.0 Implementation and Delta Validation'. ESA document ERSE-DTEX-EOAD-TN-02-0006
- Levelt, P. F., Khattatov, B. V., Gille, J. C., Brasseur, G. P., Tie, X. X. and Waters, J. W. 1998 Assimilation of MLS ozone measurements in the global three-dimensional chemistry transport model ROSE. *Geophys. Res. Lett.*, **25**, no. 24, 4493–4496
- Lyster, P., Cohn, S., Menard, R., Chang, L.-P., Lin, S.-J. and Olsen, R. G. 1997 Parallel implementation of a Kalman filter for constituent data assimilation. *Mon. Weather Rev.*, **125**, no. 7, 1674–1686
- McLinden, C. A., Olsen, S. C., Hannegan, B., Wild, O., Prather, M. J. and Sundet, J. 2000 Stratospheric ozone in 3-D models: A simple chemistry and the cross-tropopause flux. *J. Geophys. Res.*, **105**, no. D11, 14653–14665
- Meijer, Y.J., Van der A, R. J., Van Oss, R. F., Swart, D. P. J., Kelder, H. M. and Johnston, P. V. 2003 Global Ozone Monitoring Experiment ozone profile characterization using interpretation tools and lidar measurements for intercomparison. *J. Geophys. Res.*, **108**, no. D23, 4723, doi:10.1029/2003JD003498
- Menard, R. and Chang, L.-P. 2000 Stratospheric assimilation of chemical tracer observations using a Kalman filter. Part II: χ^2 -validated results and analysis of variance and correlation dynamics. *Mon. Weather Rev.*, **128**, no. 8, 2672–2686

- Munro, R., Siddans, R., Reburn, W. J. and Kerridge, B. J. 1998 Direct measurement of tropospheric ozone distributions from space *Nature*, **392**, 168-171
- Parrish, D. and Derber, J. 1992 The National Meteorological Center's spectral statistical-interpolation analysis system. *Mon. Weather. Rev.*, **120**, 1747-1763
- Riishøjgaard, L. P. 1997 On four-dimensional variational assimilation of ozone data in weather prediction models. *Q. J. R. Meteorol. Soc.*, **122**, 1545-1571
- Riishøjgaard, L. P. 1998 A direct way of specifying fbw-dependent background error correlations for meteorological analysis systems. *Tellus A*, **50**, 42-57
- Rodgers, C.D. 2000 Inverse methods for atmospheric sounding; theory and practice. World Scientific Publishing, Singapore
- Spurr, R., Thomas, W. and Loyola, D. 2002 'GOME Level 1 to 2 Algorithms Description'. Deutsches Zentrum für Luft und Raumfahrt, Germany
- Struthers, H., Brugge, R., Lahoz, W. A., O'Neill, A. and Swinbank, R. 2002 Assimilation of ozone profiles and total column measurements into a global general circulation model. *J. Geophys. Res.*, **107**, doi:10.1029/2001JD000957
- Štajner, I., Riishøjgaard, L. P. and Rood, R. B. 2001 The GEOS ozone data assimilation system: Specification of error statistics. *Q. J. R. Meteorol. Soc.*, **127**, 1069-1094
- Valks, P.J.M., PETERS, A.J.M., Lambert, J.C., Zehner, C. and Kelder, H.M. 2003 A fast delivery system for the retrieval of near-real time ozone columns from GOME data, *Int. J. Remote Sensing*, **24**, no. 3, 423-436
- Van der A, R., Van Oss, R., PETERS, A., Fortuin, J.P.F., Meijer, Y. and Kelder, H.M. 2002 Ozone profile retrieval from recalibrated Global Ozone Monitoring Experiment data. *J. Geophys. Res.*, **107**
- Van Oss, R. F., Voors, R. H. M. and R. D. J. Spurr, 2002 'Ozone Profile Algorithm'. Pp. 53-74 in *Algorithm Theoretical Baseline Document, II*, OMI Ozone Products. Ed. P. K. Bhartia, NASA Goddard Space Flight Center, Greenbelt, Maryland, U.S.A.
- WMO (World Meteorological Organization) 2003 'Scientific assessment of ozone depletion: 2002'. Global Ozone Research and Monitoring Project - Report no. 47, 498 pp, Geneva